Journal of Petroleum and Gas Engineering Vol. 4(2), pp. 35-45, February 2013
Available online at http://www.academicjournals.org/JPGE
DOI: 10.5897/JPGE12.029
ISSN 2141-2677 ©2013 Academic Journals

Full Length Research Paper

Minimizing entropy generation for louvered fins in a plate-fin compact heat exchanger

Masoud Asadi[1] and Nasrin Dindar Mehrabani[2]

[1]Department of Mechanical Engineering, Azad Islamic University Science and Research branch ,Tehran, Iran.
[2]Department of Mathematics & Computer Science, Amir Kabir University of Technology, Tehran, Iran.

Accepted 18 January, 2013

With distributed power generation market, the most economical solution today is to generate power through small gas turbine systems, arbitrarily categorized as microturbines (5 to 200 kW) orminiturbines (200 to 500 kW). The thermal efficiency of such microturbines is about 20% or less if no recuperator is used in the system but, using a recuperator operating at 87% effectiveness, the efficiency of the gas turbine system increases to about 30%, a substantial performance improvement. However, cost of the recuperator is approximately 30% of the total power plant. This means that the heat exchanger (recuperator) must be designed to get high performance with minimum cost. In this paper, after providing the necessary concise information on compact heat exchangers, the discussion is presented on minimizing entropy generation for a compact heat exchanger with Louvered fins. So, thermodynamical optimization can play a key role in providing better performance for a compact heat exchanger.

Key words: Entropy generation, plate-fin heat exchanger, louvered fin, microturbine.

INTRODUCTION

Heat exchangers play a key role on automobiles, refrigerators and air conditioning system. Nowadays, efficient heat exchangers are required in order to save energy. Aluminum-brazed heat exchanger with multi-louvered fin and flat tube is used widely in industry due to high compactness and excellent heat transfer performance. A number of experimental studies (Davenport, 1980, 1983; Achaichia, 1987; Achaichia and Cowell, 1988; Huihua and Xuesheung, 1989; Aoki et al., 1989; Rugh et al., 1992; Sunden and Svantesson, 1992; Chang et al., 1994, 1996, 1997; Kim and Bullard, 2002; Lyman et al., 2002; Zhang and Tafti, 2003; Qi et al., 2007; Dong et al., 2007) and numerical simulations (Sahnoun and Webb, 1992; Springer and Thole, 1998; Tafti et al., 1999; Leu et al., 2001; Wu and Webb, 2002) have been conducted in recent years, in heat exchangers industry.

*Corresponding author. E-mail: masoud2471@gmail.com. Tel: 00989122469837.

A schematic of a louvered fin compact heat exchanger is shown in Figure 1. When such louvered fins were first introduced, it was believed that increased heat transfer was due to added turbulence initiated by flow through the louvered array (Webb, 1991). Early flow visualization studies on scaled up louver designs quickly dispelled this theory. It was observed that as air passed through the louvers, the flow resulted in two distinct flow directions to be classified: axial (or duct) directed flow and louver directed flow. Axial flow occurs when the flow maintains the direction of the inlet flow. Louver directed flow occurs when the flow is aligned parallel to the louvers. These two directions are clearly indicated in the louvered fin cross section in Figure 2. Thus, in a strongly louver directed flow, the individual louvers essentially act as small flat plates aligned parallel to the flow (Hsieh and Jang, 2006). The explanation for increased heat transfer came from the realization that along with the new boundary layer that formed on each of these louvers came a corresponding high heat transfer coefficient (Andrew and Lyman, 2000).

Extensive studies have shown that the flow and heat

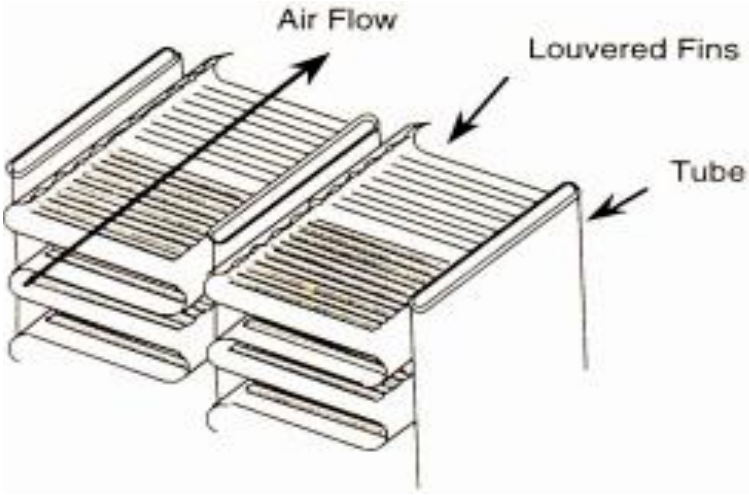

Figure 1. Schematic of a typical louvered fin-and-tube heat exchanger.

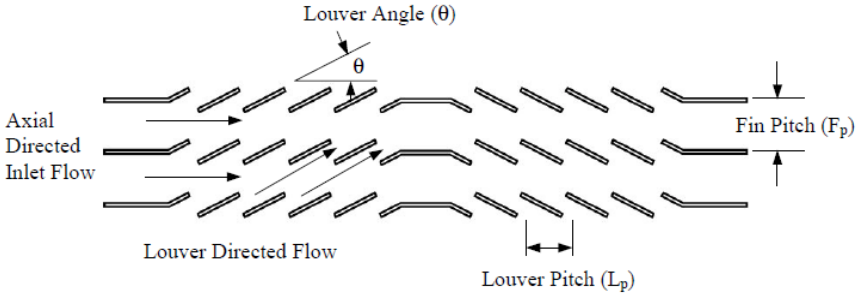

Figure 2. Side view of a typical louvered fin geometry.

transfer resulting in louvered fin arrays is quite complex. It has been shown that the degree to which the flow becomes aligned with the louvers is dependent on geometry and Reynolds number. Vortex shedding, which serves to increase heat transfer, may occur off the leading and trailing edges of the louvers. Heated wakes from louvers continue downstream and interact with downstream louvers creating complex thermal and flow field structures. The attempt to gain a detailed understanding of these mechanisms is what has been done by many researchers such as Davenport (1983) and Achachia (1988). Davenport (1983) performed overall heat transfer experiments on 32 non-standard geometries of louvered fin heat exchangers. After that, Achachia and Cowell (1988) presented experimental data of overall heat transfer and friction factor for 15 variants of louvered fin geometries. Achachia and Cowell (1988) found that at Reynolds numbers below 200, heat transfer performance flattened off considerably.

Even with the significant heat transfer enhancement of louvers, the thermal resistance on the air side of a typical fin-and-tube heat exchanger still dominates the thermal resistance of the system. The thermal resistance of the liquid side is typically 5 to 10 times lower than the thermal resistance of the air side (Yousefi and Darus, 2011: Yousefi et al., 2012). As a result, any modification that result in an increase in the air side efficiency of a heat exchanger is very valuable.

The higher level of the optimization leads to perform the thermal design of the heat exchanger, defining its operating parameters through minimization/maximization of a certain objective function like entropy generation, pressure drop or heat exchanger's costs. So besides calculating the optimized values of volume, pressure and temperature, at this level it is also possible to minimize entropy generation based on constant surface area. The second optimization level involves minimizing entropy generation based on constant volume. Furthermore, when volume and surface area are constant the thermodynamical optimization can be done by modifying Reynolds number.

In this work, the heat exchanger designing process tends to a sizing problem. So using following diagram can be useful.

THERMAL DESIGN

There are two basic types of thermal design problems: rating and sizing. In a rating problem, the geometry and size of the heat exchanger are fully specified. Also, entering flow rates and fluid temperatures are known. So, the job is to compute heat exchanger efficiency and pressure drop for each stream. However, in a sizing problem, the heat exchanger requirement is specified and the designer must calculate the heat exchanger size (Kays and London, 1984). Typically, allowable pressure drops are given for each fluid stream. A number of decisions must be made prior to making the thermal performance calculation (Kays and London, 1984)

1. Heat exchanger flow arrangement, for example, counter flow.
2. Heat exchanger materials, as influenced by fluid temperatures and corrosion potential.
3. Fin geometry and fin thickness, as influenced by design pressure requirements.
4. The type of surface geometry and fin spacing and height. Fouling considerations influence the type of surface geometry and fin spacing that may be selected. Fin height is influenced by the desired fin efficiency.
5. Heat exchanger frontal area. This key decision establishes the Reynolds number for each flow stream. The pressure losses are directly dependent on this decision.

In this work, the heat exchanger designing process tends to a sizing problem. So Figure 3 can be useful.

Since the outlet temperatures are unknown, the $\varepsilon - NTU$ is suitable, where

$$\mathrm{Q} = \varepsilon \mathrm{C}_{\min}\left(\mathrm{T}_{\mathrm{h,i}} - \mathrm{T}_{\mathrm{c,i}}\right) = \varepsilon \mathrm{C}_{\min}\Delta \mathrm{T}_{\max} \quad (1)$$

Here $\varepsilon, \Delta T_{\max}$ and $C_{\min}$ are the heat exchanger efficiency, entering temperature difference and the minimum of heat capacity respectively. ε, the heat exchanger efficiency, is a dimensionless number, and is a function of NTU and C^*:

$$\varepsilon = \phi\left(\mathrm{NTU}, \mathrm{C}^*, \text{flow arragment}\right) \quad (2)$$

Where C^* is defined by:

$$\mathrm{C}^* = \frac{\mathrm{C}_{\min}}{\mathrm{C}_{\max}} = \frac{\left(\dot{m}\mathrm{C}_{\mathrm{p}}\right)_{\min}}{\left(\dot{m}\mathrm{C}_{\mathrm{p}}\right)_{\max}} = \begin{cases} \dfrac{\left(\mathrm{T}_{\mathrm{c,o}} - \mathrm{T}_{\mathrm{c,i}}\right)}{\left(\mathrm{T}_{\mathrm{h,i}} - \mathrm{T}_{\mathrm{h,o}}\right)} & \text{for } \mathrm{C}_{\mathrm{h}} = \mathrm{C}_{\min} \\ \dfrac{\left(\mathrm{T}_{\mathrm{h,i}} - \mathrm{T}_{\mathrm{h,o}}\right)}{\left(\mathrm{T}_{\mathrm{c,o}} - \mathrm{T}_{\mathrm{c,i}}\right)} & \text{for } \mathrm{C}_{\mathrm{c}} = \mathrm{C}_{\min} \end{cases} \quad (3)$$

The other important parameter is NTU, Where it is considered as the number of transfer unit.

$$\mathrm{NTU} = \frac{\mathrm{UA}}{\mathrm{C}_{\min}} = \frac{1}{\mathrm{C}_{\min}}\int_{\mathrm{A}} \mathrm{UdA} \quad (4)$$

To calculate the outlet temperatures of both fluids, hot and cold, the – Equations (5) and (6) can be considered.

$$T_{h,o} = T_{h,i} - \varepsilon\left(\frac{C_{\min}}{C_h}\right).\left(T_{h,i} - T_{c,i}\right) \quad (5\text{-a})$$

$$T_{c,o} = T_{c,i} + \varepsilon\left(\frac{C_{\min}}{C_c}\right).\left(T_{h,i} - T_{c,i}\right) \quad (5\text{-b})$$

One of the key stage in designing a heat exchanger is accurate calculation of fluid properties. But before doing this, it is necessary to compute average temperature of each fluid. Here, according to shah research (Shah, 1981) if $C^* \geq 0.50$ the average temperatures would be

$$T_{h,m} = \frac{T_{h,i} + T_{h,o}}{2} \quad (6\text{-a})$$

$$T_{c,m} = \frac{T_{c,i} + T_{c,o}}{2} \quad (6\text{-b})$$

Else, they would be based on Table 1. Fluid properties are as shown in Table 2.

Heat transfer coefficient is calculated form j, colburn factor. Although there some equations for colburn and friction factors, Kays and London (1984) have introduced these factors versus Reynolds number.

$$h = j.G.C_P.\mathrm{Pr}^{\frac{-2}{3}} \quad (7)$$

$$G = \frac{\dot{m}}{A_{fr}} \quad (8)$$

In this formula, G and A_{fr} are mass velocity and free flow cross-sectional area respectively.

Furthermore, frictional pressure drop in both sides is given by:

$$\Delta P_1 = \frac{G_1^2}{2\rho_{in,1}}\left[\left(1 + K_{C,1} - \sigma_1^2\right) + 2\left(\frac{\rho_{in,1}}{\rho_{out,1}} - 1\right) + \left(f_1 \times \frac{S_1}{A_1} \times \frac{\rho_{in,1}}{\rho_{m,1}}\right) - \left(1 - \sigma_1^2 - k_{e,1}\right) \times \frac{\rho_{in,1}}{\rho_{out,1}}\right] \quad (9)$$

Where σ is the ratio of free flow area to the frontal area. Also, K_c and K_e are contraction and expansion coefficients.

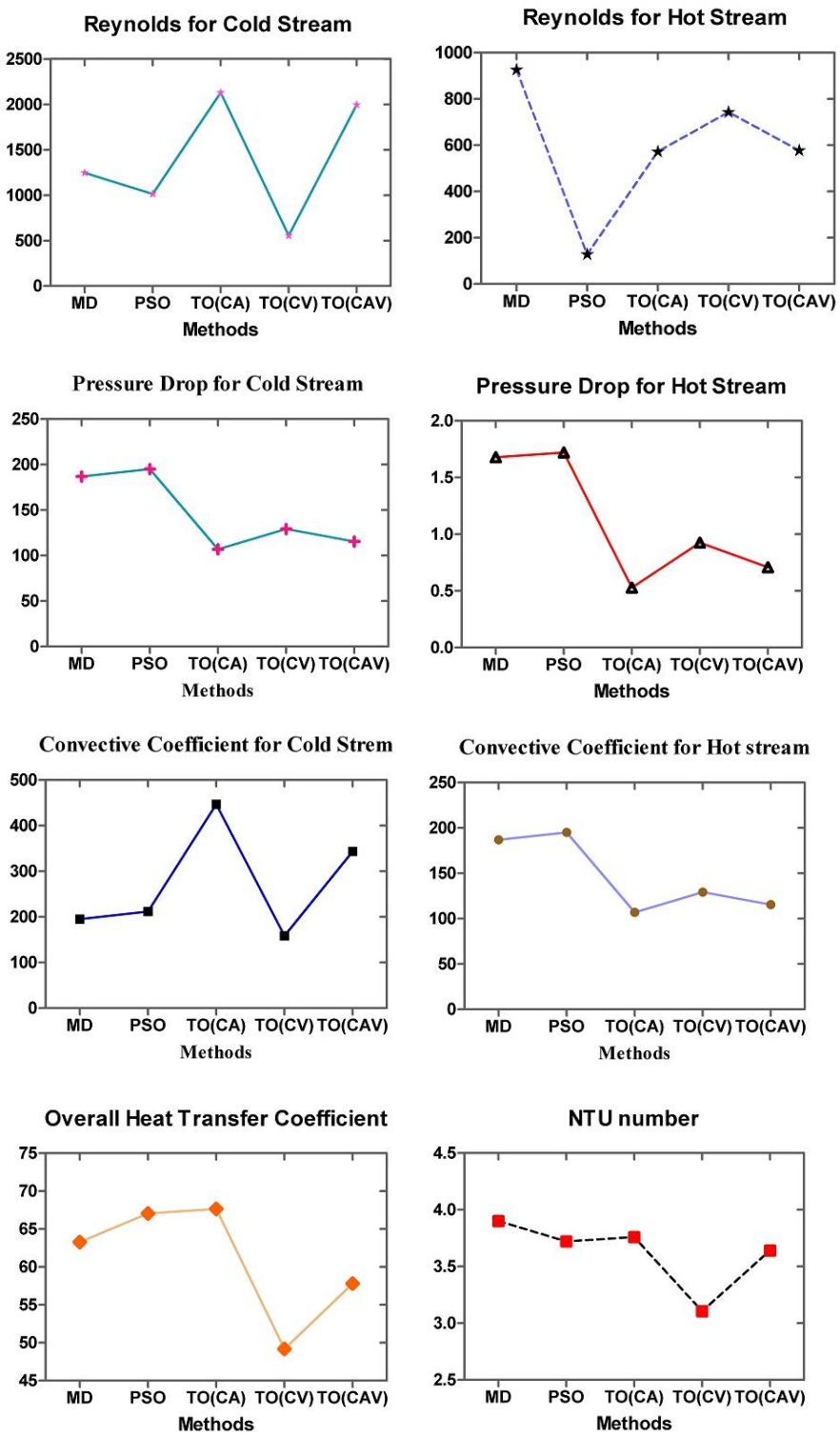

Figure 3. A comparison among the results of different methods.

ENTROPY GENERATION

The irreversibility of any heat exchanger is due to two factors; the transfer of heat across the stream – to – stream temperature difference and the frictional pressure drop. The fluid friction and heat transfer irreversibility can systematically be reduced by showing down the movement of fluid through the heat exchanger. This

Table 1. Approximate bulk mean temperature on hot and cold side of a two-fluid heat exchanger Kuppan (2000).

$C_{\max} = hot\ fluid$	$C_{\max} = cold\ fluid$
$C_{\min} = cold\ fluid$	$C_{\min} = hot\ fluid$
$T_{h,m} = \frac{T_{h,i} + T_{h,o}}{2}$	$T_{c,m} = \frac{T_{c,i} + T_{c,o}}{2}$
$T_{c,m} = T_{h,m} - \Delta T_{lm}$	$T_{h,m} = T_{c,m} + \Delta T_{lm}$
$\Delta T_{lm} = \frac{(T_{h,m} - T_{c,i}) - (T_{h,m} - T_{c,o})}{\ln[(T_{h,m} - T_{c,i}) - (T_{h,m} - T_{c,o})]}$	$\Delta T_{lm} = \frac{(T_{h,i} - T_{c,m}) - (T_{h,o} - T_{c,m})}{\ln[(T_{h,i} - T_{c,m}) - (T_{h,o} - T_{c,m})]}$

Table 2. Fluid properties.

	$\rho_i\left(\frac{Kg}{m^3}\right)$	$\rho_0\left(\frac{Kg}{m^3}\right)$	$K\left(\frac{W}{m.K}\right)$	$\mu\left(\frac{N.S}{m^2}\right)$	$C_P\left(\frac{Kj}{Kg.K}\right)$	$\frac{1}{\rho_m}$	Pr
Gas	0.399	0.491	43.9	2.88×10^{-5}	1.58	0.4182	0.683
Air	2.934	2.017	0.05	3.55×10^{-5}	1.04	2.2684	0.735

technique is synonymous with employing larger heat exchanger, that is, more heat transfer area and more heat exchanger volume (Yousef et al., 2012).

The irreversibility due to heat transfer is

$$\dot{S}_{gen} = \left(\dot{m}C_P\right)_h Ln\frac{T_{h,o}}{T_{n,i}} + \left(\dot{m}C_P\right)_c Ln\frac{T_{c,o}}{T_{c,i}} \quad (10)$$

Where entropy changes associated with the frictional pressure drops $(P_{in} - P_{out})_{h,c}$ have not been included. The entropy generation number is defined by Equation (11).

$$N_s = \frac{\dot{S}_{gen}}{\left(\dot{m}C_P\right)_{\max}} \quad (11)$$

Here it is assumed ideal gas behavior on either side of the heat exchanger surface. For Simplicity, consider a balanced counter flow arrangement $(C^* = 1)$ in which the stream – to – stream temperature difference and frictional pressure drops are not negligible. So the entropy generation rate in this arrangement is

$$\dot{S}_{gen} = \left(\dot{m}C_P\right)_h Ln\frac{T_{h,o}}{T_{n,i}} + \left(\dot{m}C_P\right)_c Ln\frac{T_{c,o}}{T_{c,i}} - \dot{m}_h R\, Ln\frac{P_{h,o}}{P_{K,i}} - \dot{m}_c R\, Ln\frac{P_{c,O}}{P_{c,i}} \quad (12)$$

Where the first two terms on the right represent the heat transfer irreversibility and the last two terms account for fluid friction. Thus, the entropy generation number becomes.

$$N_S = \frac{\tau}{NTU_h} + \frac{R}{C_P}\left(\frac{\Delta P}{P}\right)_h + \frac{\tau^2}{NTU_c} + \frac{R}{C_p}\left(\frac{\Delta P}{P}\right)_C \quad (13)$$

With

$$\tau = \frac{|T_\circ - T_i|}{(T_i T_o)^{0.5}} \quad (14)$$

The heat transfer irreversibility vanishes when the area is very large $(NTU \to \infty)$ or when the counter flow is isothermal due to end conditions $(\tau = \circ)$. Also, the fluid – friction irreversibility vanishes when the pressure drops on the two sides of the surface are zero.

The one-side irreversibility number depends on six parameters, which can be grouped in two rows:

$$\tau(T_h, T_c), \frac{R}{C_p}, \mathrm{Pr}$$
$$\frac{4L}{D}, \mathrm{Re}_D, G_* \quad (15)$$

The upper row is fixed as soon as the working fluid and two inlet conditions are specified. The second row parameter depends on the geometry of the heat – exchanger duct. For example, Re_D and G_* Can be considered as fixed, while the flow path length $\frac{4L}{D}$ is selected on the basis of minimizing the irreversibility. In actual applications one or more geometric parameters are constrained based on economic considerations. The minimization of irreversibility subject to constant area is important in cases in which the cost of building the heat transfer surface is a major component in the overall cost formula for the heat exchanger system.

The heat transfer area for one side by using the definition of hydraulic diameter is:

$$A = \frac{4L}{D} A_{fr} \tag{16}$$

Where A_{fr} is the flow cross-section. Also, this expression can be put in dimensionless form using Equation (17).

$$G_* = \frac{G}{(2\rho p)^{0.5}} \tag{17-a}$$

$$A_* = \frac{4L}{D} G_*^{-1} \tag{17-b}$$

So, when $N_{s,\min} = \frac{3}{2^{\frac{2}{3}}} \frac{\tau^{\frac{4}{3}} \mathrm{Re}_D^{\frac{1}{3}} f^{\frac{1}{3}} \left(\frac{R}{cp}\right)^{\frac{1}{3}}}{st^{\frac{2}{3}} V_*^{\frac{1}{3}}}$ and Re_D are fixed, the one-side entropy generation number can be minimized by properly selecting G_*:

$$G_{*,opt} = \left\{ \frac{\tau^2}{3A_*^2 \left(\frac{R}{c_p}\right) f\ st} \right\}^{0.25} \tag{18}$$

$$N_{s,\min} = \frac{4}{3^{\frac{3}{4}}} \frac{\tau^{\frac{3}{2}} \left(\frac{R}{C_p}\right)^{\frac{1}{4}} f^{\frac{1}{4}}}{A_*^{\frac{1}{2}} St^{\frac{3}{4}}} \tag{19}$$

These equations demonstrate that low entropy generation levels are possible only when sufficient heat transfer area is available.

Besides, the constant volume constraint governs the design of the heat exchanger for application in which space is on expensive commodity. The volume on one side of the surface is:

$$V = LA_c \tag{20-a}$$

$$V_* = \frac{4L}{D} \mathrm{Re}_D G_*^{-2} \tag{20-b}$$

So, when V_* and Re_D are specified, the minimum irreversibility design is described by:

$$G_{*,opt} = \left\{ \frac{\tau^2 \mathrm{Re}_D^2}{2f\ st \left(\frac{R}{CP}\right) V_*^2} \right\}^{\frac{1}{6}} \tag{21}$$

$$N_{s,\min} = \frac{3}{2^{\frac{2}{3}}} \frac{\tau^{\frac{4}{3}} \mathrm{Re}_D^{\frac{1}{3}} f^{\frac{1}{3}} \left(\frac{R}{cp}\right)^{\frac{1}{3}}}{st^{\frac{2}{3}} V_*^{\frac{1}{3}}} \tag{22}$$

CASE STUDY

To clarify the application of the mentioned optimization procedure, a case study taken from Oil Laboratory in Iran (Mechanical Research Group, 2006 - Report of "Design and Modeling of microturbine heat cycle" in Oil Laboratory of Iran) is considered. A gas–to–air counter flow heat- exchanger having heat duty of 100 kw is needed to be designed for the minimum surface area and volume separately. Gas and air inlet temperatures are 865 k° and 475 k° where gas and air mass flow rates are 1.4676 kg/s and 1.45 kg/s respectively. Pressure drops are set to be limited to 6.36 and 12 kpa at hot and cold side. The heat exchanger material is aluminum with density of 2700 $\frac{kg}{m^3}$. Table 3 presents the operating conditions used in thermal design. Also, louvered fin surface is used on the gas and air sides, where geometric properties of them are according to Table 4.

RESULTS AND DISCUSSION

For the prescribed heat duty and allowable pressure drop, the optimization problem is finding the design variables that minimize the entropy generation based on constant volume and constant surface area. In others word, after mechanical and thermal designing a heat

Table 3. Operating conditions.

Variable	Data
Allowable pressure drop for hot side (%)	6
Allowable pressure drop for hot side (%)	3
Outlet gas temperature(k)	694
Inlet gas temperature(k)	865
Outlet air temperature(k)	670
Inlet air temperature(k)	475
Outlet pressure from compressor(bar)	4
Outlet pressure from turbine(bar)	1.06
Gas mass flow rate (kg/s)	1.4676
Air mass flow rate(kg/s)	1.45

Table 4. Geometric Parameters of Louvered fins.

Fins	$b(mm)$	$D_h(mm)$	$\beta\left(\frac{m^2}{m^3}\right)$	$\frac{S_f}{S}$	$\delta(mm)$
$\frac{1}{2}$a – 6.06	6.35	4.453	840	0.640	0.152
$\frac{3}{8}$ – 8.7	6.35	3.650	1007	0.705	0.152

Table 5. Information about choosing a fin.

Goals	P arameters
volume	1) β 2) b
pressure drop	D_h
heat exchanger efficiency	1) $\frac{S_f}{S}$ 2) D_h
annually overall cos ts	1) D_h 2) β

exchanger, the thermodynamical optimization by modifying mass and air flow rates would be able to improve the heat exchanger performance. However, before doing this, it is necessary computing fluid properties based on average temperatures (Table 2).

When there are some limitations on surface area, the thermodynamical optimization will be doing based on constant surface area. In other words, the width and depth of heat exchanger are specified. Here, the height and fin geometric properties are the only variables. So, pursuant to objective function that can be minimum volume, costs or even weight of the heat exchanger, the height and fin geometric properties can change. To clarify this procedure it is assumed that the objective function be minimum volume, by using Particle Swarm Optimization algorithm (PSO) the total volume of heat exchanger will be optimized. But before optimization process by PSO algorithm, it is essential to select a suitable louvered fin. Table 5 gives useful information about choosing a fin.

As can be seen in this table β and b, which are total transfer area / volume between plates and the height of fin respectively, have direct impact on total volume. Hence, the heat exchanger with smaller b and larger β has smaller volume. On the other hand, when hydraulic diameter and height fin are small there is a logarithmic increase in pressure drop values.

Kays and London (1984) offer good diagrams and tables for different fins. Particle Swarm Algorithm is a heuristic optimization method which was first introduced by Kennedy and Ebehart (1995). In the basic PSO algorithm, particle swarm consists of "n" particles and the position of each particle stands for the potential solution in D-dimensional space.

Each particle can be shown by its current speed and position. So, the speed and position of each particle change according to the following equations:

$$v_{i,j}(t+1) = w\, v_{i,j}(t) + c_1 . r_1 . \left[p_{i,j}(t) - x_{i,j}(t) \right] + c_2 . r_2 . \left[p_{g,j}(t) - x_{i,j}(t) \right] \quad (23)$$

$$x_{i,j}(t+1) = x_{i,j}(t) + \Delta t\, v_{i,j}(t+1) \quad (23\text{-a})$$

Here $i = 1, 2, ..., N$ demonstrates the particles of swarm; $t = 1, 2, ..., t_{\max}$ indicates the iterations; w is considered as inertia weight factor; $v_{i,j}(t+1)$ is defined as the velocity of the i-th particle with respect to the best previous position of the i-th particle to the j-th dimension. In this formula, $p_{g,j}(t)$ is the best previous position among all the particles along the j-th dimension in iterations. Further information about PSO algorithm can be obtained from several books and papers in this area (Bai, 2010). A chaotic quantum-beha particle swarm approach applied to optimization of heat exchangers (2012); Coelho and Alotto, 2008; Mikki and Kishk, 2006; Clerc and Kennedy, 2002; Patel and Rao, 2010; Rao and Patel, 2010)

At this stage, and when mechanical and thermal designing are completed, optimization by PSO algorithm as well as thermodynamical optimization by modifying mass flow rates minimize the entropy generation.

Thermodynamical optimization tends to decrease gas flow arte and increase air flow rate, which cause to occur a dramatic increase in pressure drop, convective coefficient and Reynolds number for cold side. Although after optimization by PSO algorithm (Table 6) and then thermodynamical optimization, pressure drop have increased, rising NTU as well as decreasing 11% of volume compared with an increase of 9% costs due to pressure change is valuable. As can be observed from

Table 6. Optimization results by PSO algorithm.

Variable	MD	PSO
Fin pitch	343	343
Plate spacing (fin height) , b	6.35 mm	6.35 mm
Flow passage hydraulic diameter , D_h	3.65 mm	3.65 mm
Fin metal thickness , δ	0.152 mm	0.152 mm
Parting sheet thickness , a	0.152 mm	0.152 mm
Total sheet transfer area/volume between plates , β	1007	1007
Total heat transfer area/total volume , α	491.72	491.72
Fin area/total area , $\frac{S_f}{S}$	0.705	0.705
Contraction coefficient , σ	0.448	0.448
Thermal conductivity of fin , K	18.19	18.19
Height of heat exchanger , H	657 mm	579 mm
Width of heat exchanger , W	700 mm	700 mm
Depth of heat exchanger , D	500 mm	500 mm
Reynolds number of warmer fluid , Re_h	936	1218
Reynolds number of cooler fluid , Re_c	1247	1014
Pressure drop for warmer fluid , ΔP_h	1.68Kpa	1.72 Kpa
Pressure drop for cooler fluid , ΔP_c	0.77 Kpa	0.72 Kpa
Heat transfer coefficient for warmer fluid , h_h	187	195
Heat transfer coefficient for cooler fluid , h_c	195	212
Overall heat transfer coefficient , U	63.29	67.07
Number of transfer unit , NTU	3.9	3.72

Table 7. Optimization outcome based on constant surface area.

	$G_{*,opt}$	$N_{s,\min}$	G	$\dot{m}\left(\frac{kg}{s}\right)$
Hot fluid	12×10^{-3}	58×10^{-3}	3.66	0.78
Cold fluid	13×10^{-3}	282×10^{-3}	20.72	3.04

Table 8, PSO algorithm and thermodynamical optimization are complementary stages because modifying the heat exchanger size and fin geometric properties be done by PSO algorithm, and its thermal designing would improve by thermodynamical optimization.

Furthermore, when the volume of the heat exchanger is constant (Table 9) optimal flow rates can upgrade the heat exchanger performance. Here, similarly to constant surface area (Table 7), thermodynamical optimization is the last stage.

CONCLUSION

Mass flow rate has direct effect on the heat exchanger function, and determining optimal mass flow rate not only would optimize operating costs but also can improve the heat exchanger efficiency and the number of transfer unit. In actual application, and when surface area and volume of the heat exchanger is constant, thermodynamical optimization can be employed. Also, when the heat exchanger has been designed, thermodynamical optimization would determine optimal mass flow rates based on minimum entropy generation number (Tables 10, 11 and 12; Figure 3).

Nomenclature: $A_\circ$ surface area$\left(m^2\right)$; A_* dimensionless form of heat transfer area; b plate width; C_p specific heat $\left(\frac{J}{kg.k}\right)$; D_h hydraulic diameter(mm); E_C efficiency; f friction factor; F correction factor; V_* dimensionless form of mass velocity; A_* dimensionless

Table 8. Comparison among the results of manual designing, PSO algorithm and thermodynamical optimization.

Variable	MD	PSO	TO
Fin pitch	343	343	343
Plate spacing (fin height) , b	6.35 mm	6.35 mm	6.35 mm
Flow passage hydraulic diameter , D_h	3.65 mm	3.65 mm	3.65 mm
Fin metal thickness , δ	0.152 mm	0.152 mm	0.152 mm
Parting sheet thickness , a	0.152 mm	0.152 mm	0.152 mm
Total sheet transfer area/volume between plates , β	1007	1007	1007
Total heat transfer area/total volume , α	491.72	491.72	491.72
Fin area/total area , $\frac{S_f}{S}$	0.705	0.705	0.705
Contraction coefficient , σ	0.448	0.448	0.448
Thermal conductivity of fin , K	18.19	18.19	18.19
Height of heat exchanger , H	657 mm	579 mm	579 mm
Width of heat exchanger , W	700 mm	700 mm	700 mm
Depth of heat exchanger , D	500 mm	500 mm	500 mm
Reynolds number of warmer fluid , Re_h	936	1218	572
Reynolds number of cooler fluid , Re_c	1247	1014	2130
Pressure drop for warmer fluid , ΔP_h	1.68 Kpa	1.72 Kpa	0.53 Kpa
Pressure drop for cooler fluid , ΔP_c	0.77 Kpa	0.72 Kpa	2.55 Kpa
Heat transfer coefficient for warmer fluid , h_h	187	195	107
Heat transfer coefficient for cooler fluid , h_c	195	212	447
Overall heat transfer coefficient ,U	63.29	67.07	67.65
Number of transfer unit , NTU	3.9	3.72	3.76

Table 9. Optimization outcome based on constant volume

Fluid	$G_{*,opt}$	$N_{s,\min}$	G	$\dot{m}\left(\frac{kg}{s}\right)$
Hot fluid	16×10^{-3}	67×10^{-3}	4.76	1.018
Cold fluid	3.53×10^{-3}	244×10^{-3}	5.41	0.795

Table 10. The results of thermodynamical optimization based on constant volume.

Variable	MD
Height of heat exchanger , H	657 mm
Width of heat exchanger , W	700 mm
Depth of heat exchanger , D	500 mm
Reynolds number of warmer fluid , Re_h	743.2
Reynolds number of cooler fluid , Re_c	556
Pressure drop for warmer fluid , ΔP_h	0.925 Kpa
Pressure drop for cooler fluid , ΔP_c	0.309 Kpa
Heat transfer coefficient for warmer fluid , h_h	129.23
Heat transfer coefficient for cooler fluid , h_c	158.74
Overall heat transfer coefficient ,U	49.19
Number of transfer unit , NTU	3.105

form of surface area; V_* dimensionless form of volume; h convective coefficient $\left(\frac{W}{m^2.k}\right)$; K thermal conductivity $\left(\frac{W}{m^2.k}\right)$; m mass flow rate $\left(\frac{Kg}{s}\right)$; N heat transfer unit; N_S entropy generation number; T temperature of fluids; R_i ideal gas constant; R heat resistance; Re Reynolds number; $\dot{S}_{gen}$ entropy $\left(\frac{Kg}{m^3}\right)$; μ dynamic viscosity $\left(Pa.s\right)$; Subscripts; 1 input; 2 generation; St Stanton number; $U_\circ$ overall heat transfer coefficient; Greek symbols; ρ fluid density output; h

Table 11. Optimization outcome based on constant surface area and volume.

Fluid	Re_{opt}	$N_{s,\min}$	G	$\dot{m}\left(\frac{kg}{s}\right)$
Hot fluid	577.34	90×10^{-3}	3.69	0.787
Cold fluid	1996	234×10^{-3}	19.41	2.85

Table 12. The results of thermodynamical optimization based on constant surface area and volume.

Variable	MD
Height of heat exchanger , H	657 mm
Width of heat exchanger , W	700 mm
Depth of heat exchanger , D	500 mm
Reynolds number of warmer fluid , Re_h	577.34
Reynolds number of cooler fluid , Re_c	1996
Pressure drop for warmer fluid , ΔP_h	0.709 Kpa
Pressure drop for cooler fluid , ΔP_c	2.553 Kpa
Heat transfer coefficient for warmer fluid , h_h	115.60
Heat transfer coefficient for cooler fluid , h_c	343.53
Overall heat transfer coefficient , U	57.81
Number of transfer unit , NTU	3.64

warmer fluid; C cooler fluid; MD manual design; PSO optimization by PSO algorithm; TA thermodynamical optimization; CA constant surface area; CV constant volume; CAV constant surface area and volume.

REFERENCES

Achaichia A (1987). The performance of louvered tube-and-plate fin heat transfersurface. PhD thesis, Department of Mechanical and Production Engineering, Brighton Polytechnic.

Achaichia A, Cowell TA (1988). Heat transfer and pressure drop characteristics of flat and louvered plate fin surface. Exp. Therm. Fluid Sci. 1:147-157.

Andrew CL (2000). Spatially Resolved Heat Transfer Studies in compact heat exchanger. Master thesis, Virginia Polytechnic and State University.

Aoki H, Shinagawa T, Suga KK (1989). An experimental study of the local heat transfer characteristics in automotive louvered fins. Exp. Therm. Fluid Sci. 2:293-300.

Bai Q (2010). Analysis of particle Swarm optimization algorithm. College of Computer Science and Technology, Inner Mongolia University to nationalities, China, Tongliao, 028043.

Chang Y, Wang C, Chang W (1994). Heat transfer and flow characteristics of automotive brazed aluminum heat exchangers. ASHRAE Trans. 100(2):643-662.

Chang YJ, Wang CC (1996). Air-side performance of brazed aluminum heat exchangers. J. Enhanced Heat Transf. 3(1):15-28.

Chang YJ, Wang CC (1997). A generalized heat transfer correlation for louvered fin geometry. Int. J. Heat Mass Transf. 40(3):533-544.

Clerc M, Kennedy JF (2002). The particle swarm: Explosion, stability and convergence in a multi-dimensional complex space. IEEE Trans. Evolut. Comput. 6:58-73.

Coelho LS, Alotto P (2008). Global optimization of electromagnetic devices using an exponential quantum-behaved particle swarm optimizer. IEEE Trans. Magnetics 44:1074e1077.

Davenport CJ (1980). Heat Transfer and Fluid Flow in Louvered Triangular Ducts. Ph.D. Thesis, Department of Mechanical Engineering, Lanchester Polytechnic.

Davenport CJ (1983). Correlation for heat transfer and friction characteristics of louvered fin. AICHE Symp. Ser. 79(25):19-27.

Dong JQ, Cheng JP, Chen ZJ (2007). Heat transfer and pressure drop correlations for the multi-louvered fin compact heat exchangers. Energy Convers. Manage. 48:1506-1515.

Hsieh CT, Jang JY (2006). 3-D thermal-hydraulic analysis for louver fin heat exchangers with variable louver angle. Appl. Therm. Eng. 26:1629-1639.

Huihua Z, Xuesheung L (1989). The experimental investigation of oblique angles and interrupted plate lengths for louvered fins in compact heat exchangers. Exp. Therm. Fluid Sci. 2:100-106.

Kays WM, London AL (1984). Compact heat exchangers. McGraw Hill, Book Co, New York.

Kennedy JF, Eberhart RC (1995). Particle Swarm Optimization. Proc. IEEE Int. Conf. Neural Netw., Perth, Australia pp. 1942-1948.

Kim MH, Bullard CW (2002). Air-side thermal hydraulic performance of multi-louvered fin aluminum heat exchangers. Int. J. Refrigeration 25:390-400.

Kuppan T (2000). Heat Exchanger Design Handbook. New York ISBN:0-8247-9787-6.

Leu JS, Liu MS, Liaw JS, Wang CC (2001). A numerical investigation of louvered fin-and-tube heat exchangers having circular and oval tube configurations. Int. J. Heat Mass Transf. 44:4235-4243.

Lyman AC, Stephan RA, Thole KA, Zhang LW, Memory SB (2002). Scaling of heat transfer coefficients along louvered fins. Exp. Therm. Fluid Sci. 26:547-563.

Mechanical Research Group (2006). Report of "design and Modeling of microturbine heat cycle" in Oil Laboratory of Iran. March.

Mikki SM, Kishk AA (2006). Quantum particle swarm optimization for electro-magnetics. IEEE Trans. Antennas Propag. 54:2764-2775.

Patel VK, Rao RV (2010). Design optimization of shell-and-tube heat exchanger using particle swarm optimization technique. Appl. Therm. Eng. 30:1417-1425.

Qi ZG, Chen JP, Chen ZJ (2007). Parametric study on the performance of a heat exchanger with corrugated louvered fins. Appl. Therm. Eng. 27:539-544.

Rao RV, Patel VK (2010). Thermodynamic optimization of cross flow plate-fin heat exchanger, using a particle swarm optimization algorithm. Int. J. Therm. Sci. 49:1712-1721.

Rugh JP, Pearson JT, Ramadhyani S (1992). A study of a very compact heat exchanger used for passenger compartment heating in automobiles. ASME Symp. Ser. HTD. 201:15-24.

Sahnoun A, Webb RL (1992). Prediction of heat transfer and friction for the louver fin geometry. Int. J. Heat Mass Transf. 114:893-900.

Shah RK (1981). Compact heat exchanger design procedures. In: S. Kakac, A.E. Bergles, F. Mayinger, Heat exchangers: Thermal-hydraulic fundamentals and design pp. 495-536.

Springer ME, Thole KA (1998). Experimental design for flow field studies of louvered fins. Exp. Therm. Fluid Sci. 18:258-269.

Sunden B, Svantesson J (1992). Correlation of j- and f factors for multi louvered heat transfer surfaces. In: Proc. 3rd UK Natl. Conf. Heat Transf. pp. 805-811.

Tafti DK, Zhang LW, Wang G (1999). Time-dependent calculation procedure for fully developed and developing flow and heat transfer in louvered fin geometries. Numer. Heat Transf. Part A 35:225-249.

Wu XM, Webb RL (2002). Thermal and hydraulic analysis of a brazed aluminium evaporator. Appl. Therm. Eng. 22:1369-1390.

Yousef M, Darus AN, Mohammadi H (2012). An imperialist competitive algorithm for optimal design of plate- fin heat exchangers. 55:3178-3185.

Yousefi M, Darus AN (2011). Optimal design of plate-fin heat exchangers by particle swarm optimization. In: Fourth International Conference on Machine Vision (ICMV 2011): Computer Vision and Image Analysis; Pattern Recognition and Basic Technologies.
Yousefi M, Enayatifar R, Darus AN (2012). Optimal design of plate-fin heat exchangers by a hybrid evolutionary algorithm. Int. Commun. Heat Mass Transf. 39(2):258-263.
Zhang X, Tafti DK (2003). Flow efficiency in multi-louvered fins. Int. J. Heat Mass Transf. 46:1137-1150.